

# Global Convection Characteristics of Conical Taylor-Couette Flow with Shear-Thinning Fluids

メタデータ	言語: English 出版者: Wiley 公開日: 2022-11-21 キーワード: Conical Taylor-Couette flow, Mixing intensification, Numerical simulation, Shear-thinning fluid 作成者: 増田, 勇人, 伊與田, 浩志, 大村, 直人 メールアドレス: 所属: Osaka City University, Osaka City University, Kobe University
URL	<a href="https://ocu-omu.repo.nii.ac.jp/records/2019720">https://ocu-omu.repo.nii.ac.jp/records/2019720</a>

# Global Convection Characteristics of Conical Taylor-Couette Flow with Shear-Thinning Fluids

Hayato Masuda, Hiroyuki Iyota, Naoto Ohmura

<b>Citation</b>	Chemical Engineering Technology. 44(11); 2049-2055.
<b>Issue Date</b>	2021-11-19
<b>Type</b>	Journal Article
<b>Textversion</b>	Author
<b>Rights</b>	This is the peer reviewed version of the following article: Chemical Engineering Technology. Vol.44, Issu.11, p.2049-2055., which has been published in final form at <a href="https://doi.org/10.1002/ceat.202100236">https://doi.org/10.1002/ceat.202100236</a> . This article may be used for non-commercial purposes in accordance with Wiley Terms and Conditions for Use of Self-Archived Versions. This article may not be enhanced, enriched or otherwise transformed into a derivative work, without express permission from Wiley or by statutory rights under applicable legislation. Copyright notices must not be removed, obscured or modified. The article must be linked to Wiley's version of record on Wiley Online Library and any embedding, framing or otherwise making available the article or pages thereof by third parties from platforms, services and websites other than Wiley Online Library must be prohibited.
<b>DOI</b>	10.1002/ceat.202100236

Self-Archiving by Author(s)  
Placed on: Osaka City University

---

Dr. Hayato Masuda<sup>1,\*</sup>

Prof. Dr. Hiroyuki Iyota<sup>1</sup>

Prof. Dr. Naoto Ohmura<sup>2</sup>

### **Title of the manuscript**

Global convection characteristics of conical Taylor–Couette flow with shear-thinning fluids

### **Abstract Text**

A method to intensify the mixing process of scalar components within shear-thinning fluids was proposed. A conical Taylor–Couette flow enabled fluid elements to circulate in the entire fluid column owing to the global circulation flow (i.e., meridional flow) for keeping good local mixing within Taylor cells. The global convection and mixing characteristics were numerically investigated. The meridional flow was found to be enhanced with increasing shear-thinning. In addition, the mixing performance was evaluated using a passive tracer. Global mixing with shear-thinning fluids was promoted by the enhanced meridional flow compared with that of Newtonian fluids. Therefore, the conical Taylor–Couette apparatus could be used for intensifying mixing processes in shear-thinning fluid systems.

**Keywords:** Conical Taylor–Couette flow; Mixing intensification; Numerical simulation; Shear-thinning fluid

### **Author affiliations**

<sup>1</sup>Osaka City University, Department of Mechanical and Physical Engineering, 3-3-138 Sugimoto Sumiyoshi-ku Osaka, 558-8585, Japan.

<sup>2</sup>Kobe University, Department of Chemical Science and Engineering, 1-1 Rokkodai Nada-ku Kobe Hyogo, 657-8501, Japan.

Email corresponding author: hayato-masuda@eng.osaka-cu.ac.jp

## **1 Introduction**

The mixing of complex fluids, such as a non-Newtonian fluid, is one of the most difficult processes in the chemical, food, and pharmaceutical industries. These industries frequently involve the use of highly viscous shear-thinning fluids. When such fluids are stirred using a traditional stirred vessel, their viscosity spatially varies with the shear-rate distribution in the vessel. This viscosity distribution leads to the segregation of the fluid flow. In a laminar flow region, a highly viscous shear-thinning fluid shows relatively active fluid flow in the low-viscosity (high-shear-rate) region but inactivity in the high-viscosity (low-shear-rate) region. In other words, the fluid flow is limited to the high-shear-rate region. As a result, in a stirred vessel, a cavern often forms around the impeller [1]. Some studies have provided a practical correlation equation to predict various characteristics such as the cavern size and power consumption [2, 3]. Further, a novel mixer could mitigate the segregation of the fluid flow. For example, in order to destroy the cavern, Pakzad et al. [4] reported an energy-efficient coaxial mixer for non-Newtonian fluid mixing. However, Ohmura et al. [5] noted that cavern formation in the stirred vessel is unavoidable unless excess energy is injected by the impeller to make the fluid circulate through the whole region. Thus, the process design of non-Newtonian fluid mixing needs to be revolutionized to be made sustainable.

---

In industries that frequently involve non-Newtonian fluid mixing, the sophisticated control of the internal structure of final products, rather than complete homogenization, is desirable. Therefore, a gentle mixing process must be developed. A Taylor–Couette flow, that is, the flow between coaxial cylinders with the inner one rotating, can be used for realizing gentle and effective mixing. Above a critical Reynolds number ( $Re$ ) in the circumferential direction, pairs of counterrotating toroidal vortices (i.e., Taylor cells) spaced regularly along the axis appear. Mixing and heat/mass transfer are enhanced by the toroidal motion within Taylor cells. In addition, all cells move in a single line without breakdown if a relatively small axial flow is added, that is, all fluid elements undergo the same process (Taylor–Couette–Poiseuille flow) [6]. Therefore, a Taylor–Couette flow can be used as a continuous ideal plug flow reactor. Accordingly, many studies have tried to intensify various processes using a Taylor–Couette flow reactor, including polymerization [7], enzymatic reaction [8, 9], heat sterilization [10] and gas–liquid contactor [11].

A Taylor–Couette flow is suitable for not only a continuous reactor but also a batch-type mixing device. Unlike in a traditional stirred vessel, a locally high shear force is not imposed, making a Taylor–Couette flow beneficial for bioprocesses such as the cultivation of animal cells [12]. Masuda et al. [13] noted that the shear-rate distribution in a Taylor–Couette flow apparatus is much narrower than that in a stirred vessel. As a result, in a non-Newtonian fluid system, a viscosity distribution that reduces the mixing efficiency is suppressed. Thus, a Taylor–Couette flow could serve as an excellent batch-type mixing device for non-Newtonian fluid processes with shear-sensitive materials. Unfortunately, a Taylor–Couette flow prevents global mixing within the reactor because of a mass transfer barrier by each inflow boundary when it is used as a batch-type mixing device [14]. This disadvantage can be overcome by using a conical Taylor–Couette flow. In such a flow, the centrifugal force changes axially and increases with the conical radius. This axially distributed centrifugal force results in a three-dimensional basic flow circulating within the apparatus, also called a meridional flow. Wimmer [15] reported that the fluid is discharged at the largest radius, moves down in spirals to the smallest radius near the stationary shell, and returns to the largest radius near the rotating cone. The large circulation enhances global mixing at even a low  $Re$ , thus maintaining good local mixing performance within Taylor cells when used as a batch reactor for polymerization or biochemical processes [16]. Furthermore, in a non-Newtonian fluid system, the large circulation is expected to prevent the localization of the mixing or unmixing region. Therefore, the mixing performance of a conical Taylor–Couette flow with non-Newtonian fluids must be investigated further.

The present study aims to numerically investigate the characteristics of a conical Taylor–Couette flow with shear-thinning and the mixing performance based on passive scalar transport. A numerical simulation is quite useful for understanding detailed information of fluid flow and mixing. Furthermore, to develop a mixing device using a conical Taylor–Couette flow, the geometry, including the apex angle, should be optimized. However, it is difficult to experimentally realize systems with various apex angles and parameters owing to experimental costs. Thus, as preliminary study, a numerical simulation is performed.

## 2. Numerical Simulation

### 2.1. Computational Domain and Governing Equations

Figure 1 shows the computational domain. The minimum radii of the inner and outer conical cylinders were fixed as  $R_{il} = 0.024$  m and  $R_{ol} = 0.032$  m, respectively, at the bottom of the domain. The height of the conical cylinder,  $H$ , was 0.125 m. The gap width between conical cylinders,  $d$ , was kept constant at 0.008 m. The apex angle,  $\alpha$ , was varied from  $0^\circ$  to  $12^\circ$ . As a result, the maximum radii of the inner and outer conical cylinders at the top of the domain varied as  $R_{ih} = 0.024$ – $0.0506$  m and  $R_{oh} = 0.032$ – $0.0586$  m,

respectively. Here,  $\alpha = 0^\circ$  corresponds to the coaxial cylinder configuration. The radius ratio,  $\varepsilon$ , was varied from 0.75 at the top to 0.84 at the bottom along the axis.

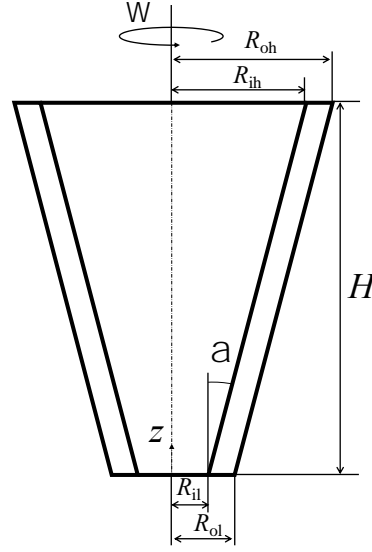


Figure 1 Computational domain.

To clarify the characteristics of global convection in a conical Taylor–Couette flow, the governing equations, namely, the mass and momentum conservation equations given below, were solved numerically.

$$\nabla \cdot \mathbf{u} = 0 \quad (1)$$

$$\frac{\partial \mathbf{u}}{\partial t} + (\mathbf{u} \cdot \nabla) \mathbf{u} = -\frac{\nabla p}{\rho} + \frac{1}{\rho} \nabla \cdot (2\eta \mathbf{D}) + \mathbf{g} \quad (2)$$

where  $\mathbf{u}$  is the velocity;  $t$ , the time;  $p$ , the pressure;  $\rho$ , the density;  $\eta$ , the viscosity;  $\mathbf{D} = (\nabla \mathbf{u} + \nabla \mathbf{u}^T)/2$ , the deformation rate tensor; and  $\mathbf{g}$ , the gravitational acceleration. In addition, the global convection characteristics of a conical Taylor–Couette flow were investigated by solving a tracing passive scalar transport, as shown in Eq. (3):

$$\frac{\partial C}{\partial t} + \mathbf{u} \nabla C = \nabla (D_s \nabla C) \quad (3)$$

where  $C$  is the scalar concentration and  $D_s$ , the diffusion coefficient of the species  $s$ . After the developed flow field was obtained by solving Eqs (1) and (2), Eq. (3) was solved including Eqs. (1) and (2). Notably, a completely developed flow field was used as the initial flow field for investigating the scalar transport.

For shear-thinning fluids, the viscosity depends on the shear rate,  $\dot{\gamma}$ , that is defined as  $\dot{\gamma} = \sqrt{2\mathbf{D}:\mathbf{D}}$ , which is the second invariant of the rate-of-strain tensor. Here, the sign must be selected such that  $\dot{\gamma}$  is positive. As a rheological model, the Carreau model was selected to characterize the apparent viscosity as a function of the shear-rate as follows [17]:

$$\eta = \eta_0 [1 + (\beta \cdot \dot{\gamma})^2]^{(n-1)/2} \quad (4)$$

where  $\eta_0$  is the zero shear-rate viscosity;  $\beta$ , the characteristic time; and  $n$ , the power-law exponent. Figure 2 shows the rheological property of the fluids used in this study.  $\eta_0$  and  $\beta$  were set as 0.05 Pa·s and 1 s, respectively. The  $n$  value indicates the slope of decreasing viscosity with the shear rate and is important for characterizing the shear-thinning behavior. Thus,  $n$  was varied from 1 to 0.3. Here,  $n = 1$  corresponds to a Newtonian fluid.

In addition, Noui-Mehidi [18] noted that the flow pattern of a conical Taylor–Couette flow is significantly affected by the acceleration speed of the inner cone. Although the effect of the acceleration speed should be taken into consideration, the rotating speed of the inner cone reached a set speed immediately in the simulation. Therefore, the acceleration rate,  $\alpha_c$ , was assumed to be infinite in this study.

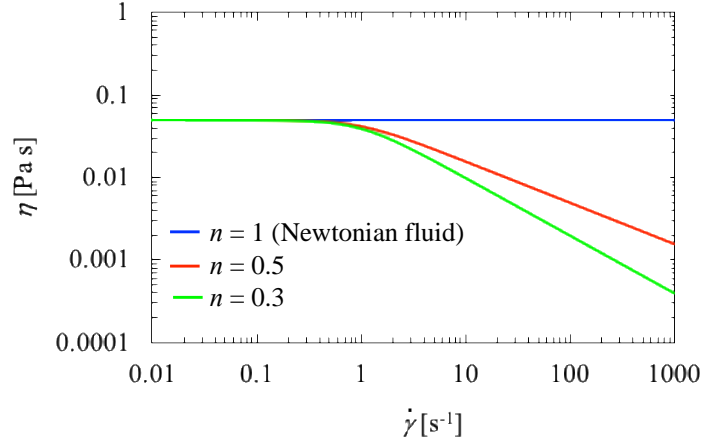


Figure 2 Rheological properties of fluids used in this study.

## 2. 2. Numerical Method and Validation

To solve the governing equations, OpenFOAM<sup>®</sup>4.1 code was utilized. The governing equations were discretized based on a finite volume method. The Crank–Nicolson scheme was used for time advancement. The second-order central difference was applied to the viscous and convective terms. Srinivasan et al. [19] noted that the use of the total variation diminishing (TVD) property to eliminate numerical oscillations with high-order differencing schemes is preferable for discretizing the convective term in Eq. (3). Therefore, the TVD scheme with van Leer’s limiter was applied to the convective term in Eq. (3). The semi-implicit method for pressure-linked equations (SIMPLE) method was used for pressure-velocity coupling.

The simulation code based on the above procedure has already been validated for a cylinder Taylor–Couette flow by authors [13]. Additionally, the flow pattern 30 s after the start of the rotation of the inner cone was compared between the experiment and the simulation at  $\alpha = 8^\circ$ , as shown in Fig. 3. Figure 3(a) and (b) show the flow visualization using a 40 wt% glycerol aqueous solution (Newtonian fluid) with Al flakes and the velocity vector in the ( $x$ - $z$ ) plane obtained through numerical simulation, respectively. In the simulation, the physical properties of 40 wt% glycerol aqueous solution were used. In both cases,  $Re$  at the top surface,  $Re|_{\text{top}}$ , was set at 160. Here,  $Re|_{\text{top}}$  was defined as follows:

$$Re|_{\text{top}} = \frac{\rho \omega R_{\text{ih}} d}{\eta} \quad (5)$$

where  $\omega$  is the rotational speed of the inner cone. In this flow system,  $Re$  actually varies axially. In this study, the flow condition was considered based on  $Re|_{\text{top}}$  because the centrifugal force at the top seems most dominant in this flow system. Actually, the instability occurs from the top [14]. In addition, the definition of  $Re$  in a shear-thinning fluid system is more complicated because of the local distribution of viscosity caused by the shear-thinning property. From a practical viewpoint, the effective  $Re$ ,  $Re_{\text{eff}}$ , based on the effective viscosity,  $\eta_{\text{eff}}$ , should be defined. To estimate  $\eta_{\text{eff}}$ , the effective shear-rate,  $\dot{\gamma}_{\text{eff}}$ , in the flow system must be estimated accurately. In this study,  $\dot{\gamma}_{\text{eff}}$  at the top,  $\dot{\gamma}_{\text{eff}}|_{\text{top}}$  was simply defined as

$$\dot{\gamma}_{\text{eff}}|_{\text{top}} = \frac{\omega R_{\text{ih}}}{d} \quad (6)$$

$\eta_{\text{eff}}$  is calculated by substituting  $\dot{\gamma}_{\text{eff}}$  into  $\dot{\gamma}$  in Eq. (4). It is noted that the estimation of effective viscosity from the detailed viscosity distribution will be necessary for the optimum design of conical Taylor–Couette flow process in the future.

Figure 3 confirmed that there were seven pairs of Taylor vortices in both cases. Thus, the simulation code used in this study was quantitatively validated even for a conical Taylor–Couette flow. The acceleration rate ( $\alpha_c$ ) was also assumed to be infinite in the experiment as well as the simulation.

Figure 4 shows the dependence of the mesh number on the velocity distribution at the middle of the gap along the axis. The velocity distribution 30 s after the start of the rotation of the inner cone for  $Re|_{\text{top}} = 200$  and  $\alpha = 8^\circ$  was used for verification. Each peak corresponds to the outflow from the inner cone toward the outer one. The dependence was checked using  $20 \times 80 \times 88$  (system-1),  $28 \times 112 \times 124$  (system-2), and  $32 \times 120 \times 140$  (system-3) meshes in the radial, circumferential and axial directions, respectively, with a Newtonian fluid for  $Re|_{\text{top}} = 140$ . System-2 and -3 did not show a significant difference. Thus, system-2 was selected owing to the reduced calculation time.

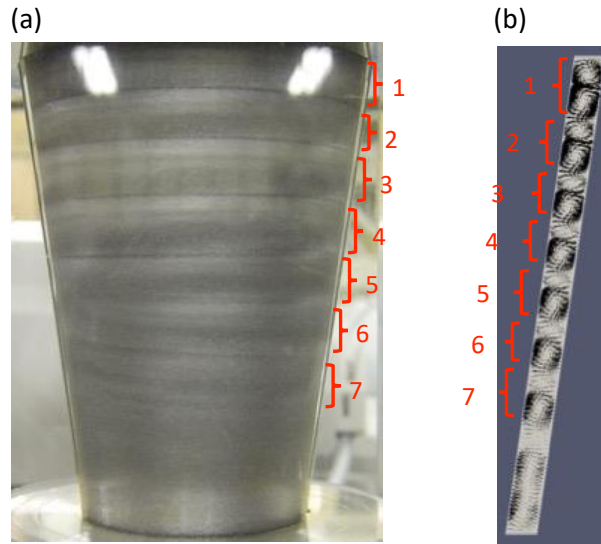


Figure 3 Comparison of (a) experimental and (b) numerical results at  $Re|_{\text{top}} = 160$ : (a) flow pattern visualized with aluminum flakes and (b) velocity vectors in the  $(x-z)$  plane. In both cases, seven pairs of Taylor vortices were observed.

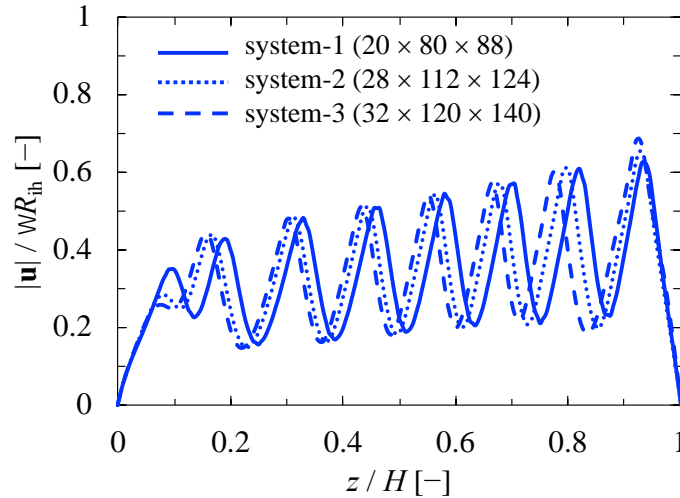


Figure 4 Dependence of mesh number on velocity distribution 30 s after the start of the rotation of the inner cone at the middle of the gap along the axis:  $Re|_{\text{top}} = 200$  and  $\alpha = 8^\circ$ .

### 3. Results and Discussion

The apex angle significantly affects the flow dynamics of a conical Taylor–Couette flow. Figure 5 shows the effect of the apex angle ( $\alpha = 0^\circ, 8^\circ, 12^\circ$ ) on the velocity distribution at  $Re|_{\text{top}} (Re_{\text{eff}}|_{\text{top}}) = 140$  for a Newtonian and shear-thinning fluid ( $n = 0.5$ ). Figure 5 mainly suggests two practically important points. First, the velocity distributions in both fluids resemble each other for each apex angle. Therefore, the flow pattern can be maintained even for a shear-thinning fluid considering  $Re_{\text{eff}}|_{\text{top}}$ . Thus, selecting  $\omega R_{\text{ih}}/d$  as the representative shear rate is considered rational. Second, the increase in the apex angle was found to retard the development of Taylor vortices in the entire apparatus. In particular, retardation was observed at the lower part where the centrifugal force is smaller. This implies that a higher centrifugal force (i.e., rotational speed of inner cone), which is not preferable for energy-saving and shear-sensitive materials, is required for the full development of Taylor vortices. Thus, a moderate angle ( $\alpha = 8^\circ$ ) was selected for further investigating the flow and mixing characteristics.

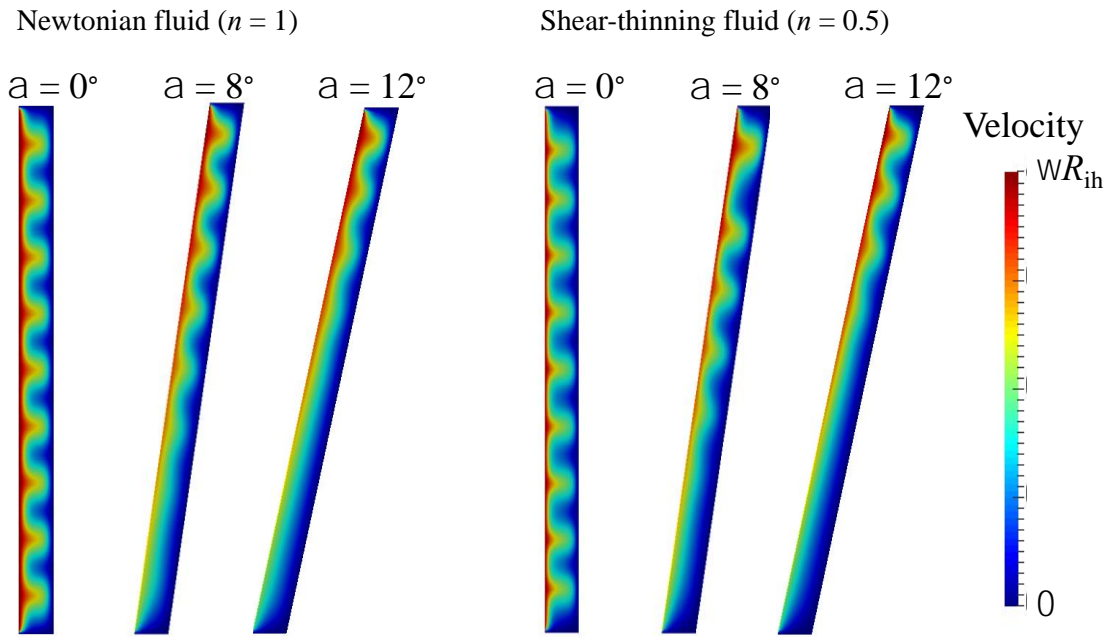


Figure 5 Effect of apex angle on velocity distribution 30 s after the start of the rotation of the inner cone in Newtonian and shear-thinning fluids at  $Re|_{\text{top}} (Re_{\text{eff}}|_{\text{top}}) = 140$ . In each figure, the left and right sides correspond to the inner and outer cone (cylinder) surfaces, respectively.

As mentioned in the introduction, the characteristics of global convection induced by a meridional flow need to be clarified. Figure 6 shows the velocity distribution in the middle of the gap along the axis at  $t = 20$  and  $30$  s for a shear-thinning fluid ( $n = 0.5$ ) and  $Re_{\text{eff}}|_{\text{top}} = 200$ . Each peak was found to shift from the bottom to top during  $10$  s. Thus, an upward motion of Taylor cells, which is induced by the meridional flow, was observed during the start-up of the inner cone (i.e.,  $\alpha_c = \infty$ ). Although studies have reported on the effect of the acceleration on the flow mode [18, 20], the case of  $\alpha_c = \infty$  is not understood. Only upward motion was observed under the simulation conditions in this study. The velocity of upward motion,  $V_t$ , was calculated as follows:

$$V_t = \frac{\Delta H}{\cos(\alpha/\pi)} \frac{1}{\Delta t} \quad (7)$$

where  $\Delta H$  is the shift distance of each peak in the axial direction during  $\Delta t$ . Strictly,  $\Delta H$  slightly differs for each peak. Thus, the third peak from the top was selected, because the Taylor cells adjacent to the end

plate were significantly affected by the Ekman boundary layer [21]. Figure 7 shows the effect of rheological properties on the upward velocity at  $Re|_{\text{top}}$  ( $Re_{\text{eff}}|_{\text{top}}$ ) = 140, 200, and 300. Notably, the velocity was normalized by the rotating velocity of the inner cone. The normalized velocity decreased with an increase in  $Re|_{\text{top}}$  ( $Re_{\text{eff}}|_{\text{top}}$ ) owing to the immobilization of Taylor cells by the higher centrifugal force suppressing the meridional flow. For each  $Re|_{\text{top}}$  ( $Re_{\text{eff}}|_{\text{top}}$ ), the upward velocity was clearly enhanced with an increase in the shear-thinning property. The driving force of meridional flow is the difference of  $Re$  at the top and bottom [15].  $Re$  at the bottom,  $Re|_{\text{bottom}}$ , was defined as follows:

$$Re|_{\text{bottom}} = \frac{\rho\omega R_{\text{ih}}d}{\eta} \quad (8)$$

Besides, the effective shear-rate at the bottom,  $\dot{\gamma}_{\text{eff}}|_{\text{bottom}}$ , was defined as follows:

$$\dot{\gamma}_{\text{eff}}|_{\text{bottom}} = \frac{\omega R_{\text{ih}}}{d} \quad (9)$$

For example, when  $Re$  ( $Re_{\text{eff}}$ ) = 200 at the top,  $Re|_{\text{bottom}}$  ( $Re_{\text{eff}}|_{\text{bottom}}$ ) was 114 ( $n = 1$ ), 86 ( $n = 0.5$ ) and 77 ( $n = 0.3$ ), respectively. In each fluid,  $Re$  ( $Re_{\text{eff}}$ ) monotonically increased with the axial position. Clearly, the difference between  $Re|_{\text{top}}$  and  $Re|_{\text{bottom}}$  increased with increasing the shear-thinning property. Thus, it is considered that the meridional flow was enhanced with the increase in the shear-thinning property.

Although the detailed mechanism of this enhancement is worth investigating, it would be quite useful to prevent the formation and localization of an inactive mixing region, which is often observed in a traditional stirred vessel, from a practical viewpoint. In other words, global mixing is expected to be improved in the shear-thinning fluid system when using the conical Taylor–Couette flow apparatus.

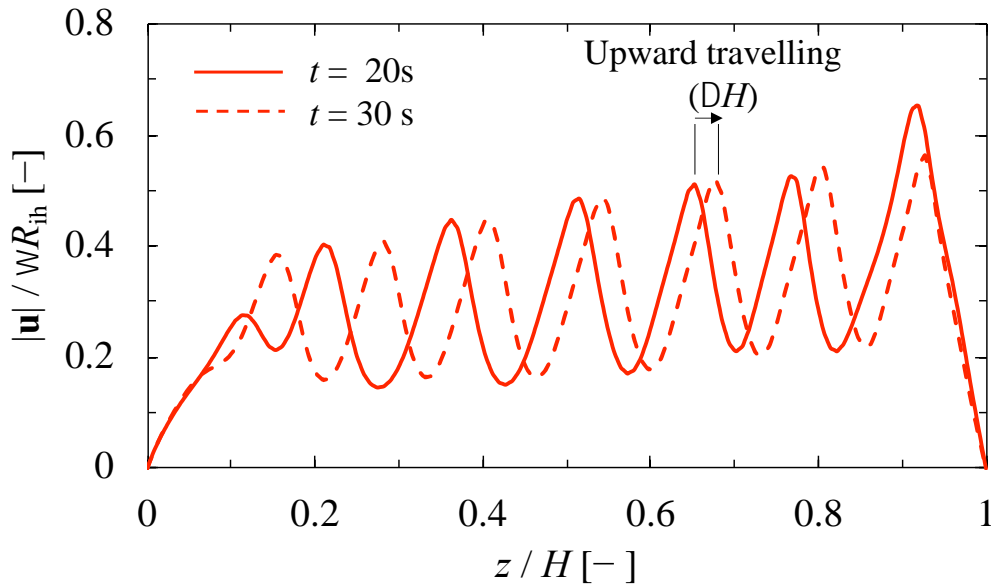


Figure 6 Velocity distribution in the middle of the gap along the axis for  $Re_{\text{eff}}|_{\text{top}} = 200$  and  $n = 0.5$ . The velocity peak was confirmed to shift upward between  $t = 20$  and 30 s.

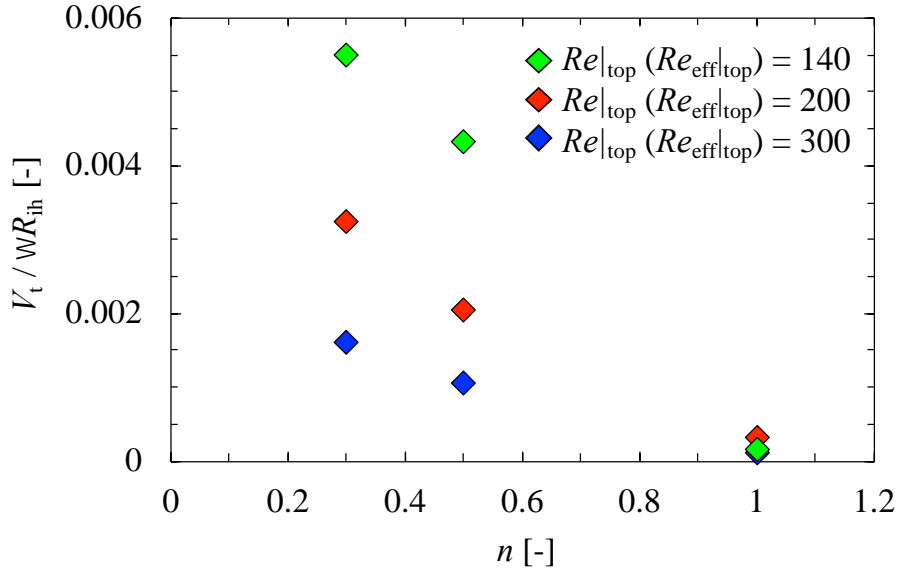


Figure 7 Effect of shear-thinning property ( $n$ ) on the normalized velocity of the upward motion of a Taylor cell.

In this study, the global mixing characteristics were numerically investigated using a passive tracer. As the initial condition, the tracer was set only at the lower half of the apparatus. Further, the velocity field 30 s after the start of the rotation of the inner cylinder or cone was used as the initial velocity to eliminate the effect of flow development on the global mixing. For example, Figure 8 shows a comparison of the tracer diffusion process with time between (a) cylindrical ( $\alpha = 0^\circ$ ) and (b) conical ( $\alpha = 8^\circ$ ) systems in the scalar concentration field for  $Re_{eff|_{top}} = 200$  at  $n = 0.3$ . The concentration field is shown in the ( $x$ - $z$ ) plane. The time was made dimensionless with  $d/\omega R_{ih}$  as a reference of the time scale as follows:

$$t^* = \frac{t}{d/\omega R_{ih}} \quad (10)$$

where  $t^*$  is the non-dimensional time. The diffusion coefficient,  $D_s$ , was set at  $1.3 \times 10^{-8} \text{ m}^2 \text{ s}^{-1}$  (this is a virtual value). Strictly, the diffusion coefficient of mass should be much smaller. According to Hubacz et al. [22], the value of  $D_s$  in the liquid state is on the order of  $10^{-10} - 10^{-13} \text{ m}^2 \text{ s}^{-1}$  depending on the liquid viscosity. However, the smaller the diffusion coefficient, the finer is the required mesh size. To reduce the calculation load, the diffusion coefficient was set as on the order of  $10^{-7} - 10^{-8} \text{ m}^2 \text{ s}^{-1}$ . It is noted that the oscillation of scalar field by numerical diffusion was no observed. Figure 8 confirms that the tracer diffusion in the axial direction was prevented by the inflow boundary in the cylindrical case. This tendency corresponds to the experimental results [14]. In the conical case, the tracer was axially transported by the meridional flow and local mixing occurred favorably. Thus, the conical Taylor–Couette flow apparatus exhibits excellent performance for both global and local mixing. Fig. 9 shows the transport process of the tracer in each fluid for  $t^* =$  (a) 2,340 and (b) 6,200 at  $Re_{top} (Re_{eff|_{top}}) = 200$  in the ( $x$ - $z$ ) plane. To unify the effect of convective transport on diffusive transport in each fluid, the Peclet number ( $Pe$ ) was set at  $1.9 \times 10^4$ .  $Pe$  is defined as follows:

$$Pe = Re \cdot Sc \quad (11)$$

where  $Sc (= \eta/\rho \cdot D_s)$  is the Schmidt number. In shear-thinning fluids, an effective  $Pe$ ,  $Pe_{eff}$ , was defined based on  $Re_{eff|_{top}}$  and an effective  $Sc$ ,  $Sc_{eff}$ . Figure 9 (a) confirms that at  $t^* = 2,340$ , a lump of tracer is axially transported for shear-thinning fluids ( $n = 0.5$  and  $0.3$ ). This promotion of transport is explained by the enhanced global circulation with shear-thinning fluids, as shown in Fig. 7. In addition, the scalar concentration of the lump for  $n = 0.3$  seemed slightly higher than that for  $n = 0.5$ . Figure 9 (b) suggests

that the distribution of the tracer concentration for shear-thinning fluids was more uniform than that for Newtonian fluids.

To quantitatively investigate the mixing performance, a distributive mixing efficiency,  $M$ , is evaluated based on the standard deviation of the concentration distribution as follows [23, 24].

$$M = 1 - \frac{1}{\bar{C}} \left( \frac{1}{V} \int (C - \bar{C})^2 dV \right)^{1/2} \quad (12)$$

where  $\bar{C}$  is the mean concentration when mixing is perfect and  $V$  is the volume of the apparatus. The value of  $M$  varies from 0 for no mixing to 1 for perfect mixing. Figure 10 shows the mixing efficiency at  $Re_{\text{eff}}|_{\text{top}} = 200$  as a function of the non-dimensional time ( $t^*$ ). As clearly shown in Fig. 10, the mixing efficiency was enhanced in shear-thinning systems. For example, at  $t^* = 6,200$ , the mixing efficiency increased by 15% at  $n = 0.5$  compared with that of Newtonian fluid. Therefore, the conical Taylor–Couette flow apparatus can be considered suitable for enhancing the mixing of scalar components within shear-thinning fluids.

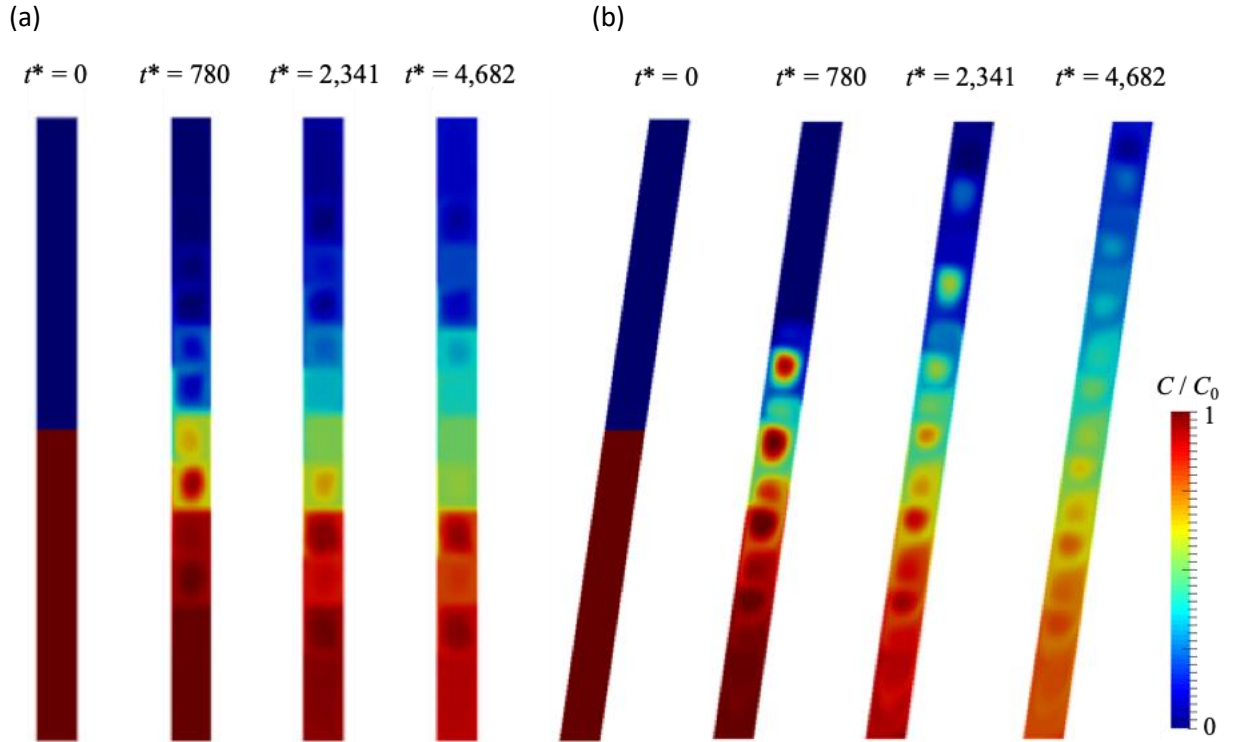


Figure 8 Passive scalar transport with time at  $Re_{\text{eff}}|_{\text{top}} = 200$  and  $n = 0.3$ : (a) cylindrical ( $\alpha = 0^\circ$ ) and (b) conical ( $\alpha = 8^\circ$ ) systems. In each figure, the left and right sides correspond to the inner and outer cone (cylinder) surfaces, respectively.

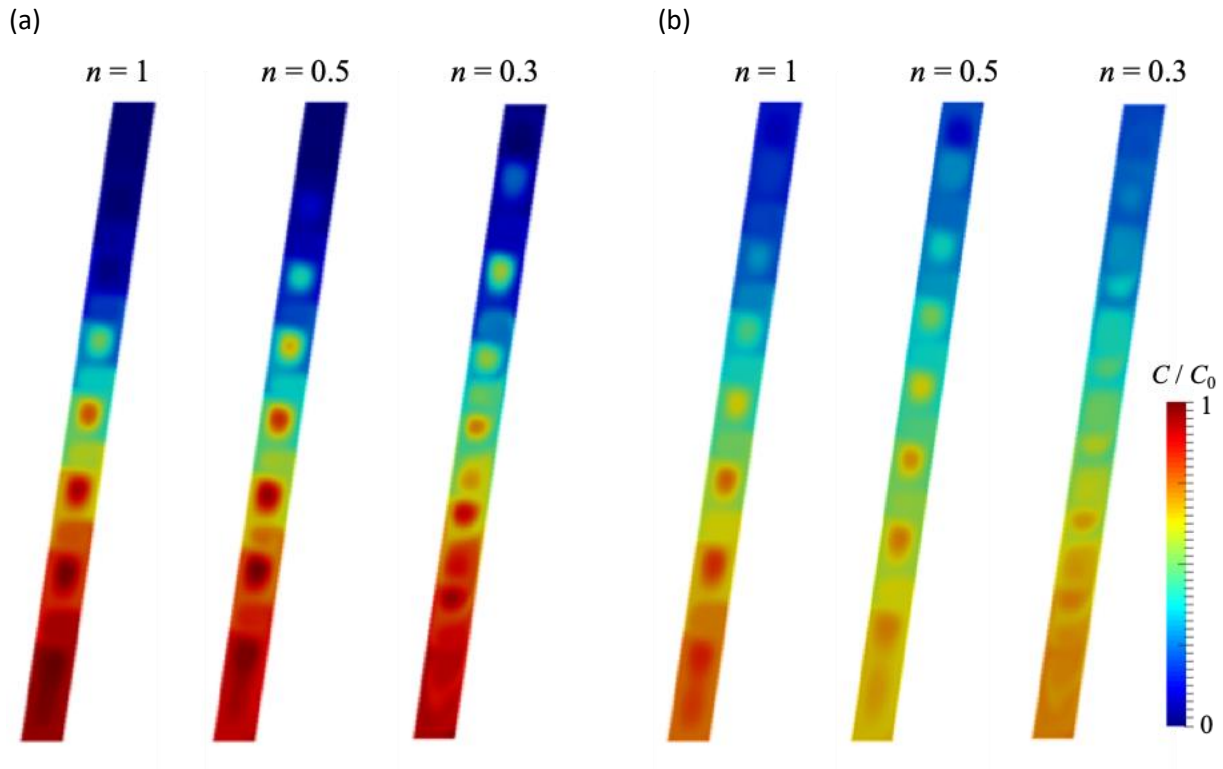


Figure 9 Effect of shear-thinning property ( $n$ ) on passive scalar transport at  $Re|_{\text{top}}$  ( $Re_{\text{eff}}|_{\text{top}}$ ) = 200 in a conical system ( $\alpha = 8^\circ$ ):  $t^* =$  (a) 2,340 and (b) 6,200. In each figure, the left and right sides correspond to the inner and outer cone (cylinder) surfaces, respectively.

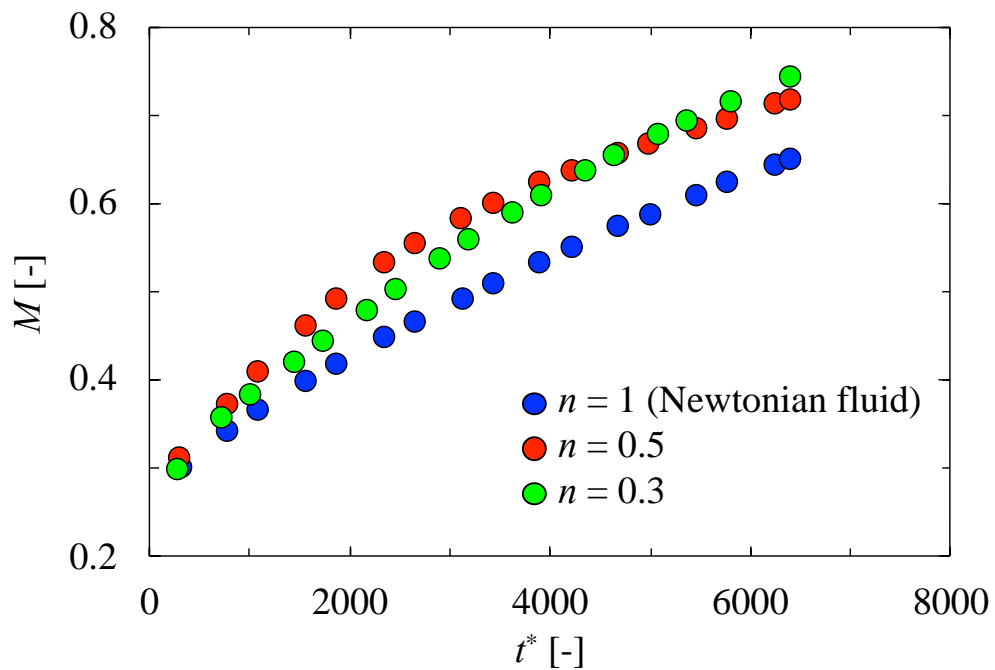


Figure 10 Distributive mixing efficiency as a function of the non-dimensional time ( $t^*$ ) in each fluid system at  $Re|_{\text{top}}$  ( $Re_{\text{eff}}|_{\text{top}}$ ) = 200.

---

#### 4. Conclusions

The global convection and mixing characteristics in a conical Taylor–Couette flow with shear-thinning fluids were numerically investigated in this study. An increase in the apex angle reduced the development of Taylor vortices, and consequently, a higher energy input and centrifugal force were required for filling Taylor cells in the entire fluid column region. In other words, a moderate apex angle was preferable in a mixing device. Thus, a system with an apex angle of  $8^\circ$  was selected for further investigation.

The upward motion of Taylor cells induced by a meridional flow, a basic conical Taylor–Couette flow, was observed in a condition that is considered the sudden start of the inner cone. In addition, the travelling velocity increased with increasing the shear-thinning property. As a result, the global mixing caused by the upward motion is enhanced was shear-thinning fluid systems. To clarify the effect of upward motion on global mixing, passive scalar transport was investigated. The results showed that, in shear-thinning fluids, the scalar was axially transported more quickly with good local mixing compared to the case of a Newtonian fluid. This tendency was quantitatively confirmed using a distributive mixing efficiency. Therefore, the conical Taylor–Couette flow could intensify mixing processes in shear-thinning fluid systems.

#### Acknowledgement

This research was partially supported by JSPS KAKENHI grant numbers JP18H03853, JP19KK0127, and JP21K14450. The authors would like to thank Mr. Katsuki Muranishi from Kobe University, Japan, for assistance with the flow visualization experiments.

#### Symbols used

$C$	[g m <sup>-3</sup> ]	scalar concentration
$C_0$	[g m <sup>-3</sup> ]	initial scalar concentration
$\bar{C}$	[g m <sup>-3</sup> ]	mean concentration
$\mathbf{D}$	[s <sup>-1</sup> ]	rate of deformation tensor
$d$	[m]	gap width
$D_s$	[m <sup>2</sup> s <sup>-1</sup> ]	diffusion coefficient
$g$	[m s <sup>-2</sup> ]	gravitational acceleration
$H$	[m]	height
$\Delta H$	[m]	shift difference of velocity peak
$n$	[–]	model parameter
$p$	[Pa]	pressure
$Pe$	[–]	Peclet number
$Pe_{\text{eff}}$	[–]	effective Peclet number
$Re$	[–]	Reynolds number
$Re_{\text{eff}}$	[–]	effective Reynolds number

---

$R_{ih}$	[m]	inner cylinder or cone at top
$R_{il}$	[m]	inner cylinder or cone at bottom
$R_{oh}$	[m]	outer cylinder or cone at top
$R_{ol}$	[m]	outer cylinder or cone at bottom
$s$	[-]	species
$Sc$	[-]	Schmidt number
$Sc_{eff}$	[-]	effective Schmidt number
$t$	[s]	time
$t^*$	[-]	non-dimensional time
$\mathbf{u}$	[m s <sup>-1</sup> ]	velocity
$V$	[m <sup>3</sup> ]	volume
$V_t$	[m s <sup>-1</sup> ]	travelling velocity of Taylor cells
$x$	[-]	coordinate
$z$	[-]	coordinate

#### Greek letters

$\alpha$	[°]	apex angle
$\alpha_c$	[rad s <sup>-2</sup> ]	angular acceleration of inner cone
$\beta$	[-]	model parameter
$\varepsilon$	[-]	radius ratio
$\dot{\gamma}$	[s <sup>-1</sup> ]	shear-rate
$\eta$	[Pa s]	apparent viscosity
$\eta_0$	[Pa s]	zero shear-rate viscosity
$\rho$	[kg m <sup>-3</sup> ]	density
$\omega$	[rad s <sup>-1</sup> ]	angular velocity of inner cone

#### Subscripts

bottom bottom plate

top top plate

#### References

- [1] P. E. Arratia, J. Kukura, J. Lacombe, F. J. Muzzio, *AIChE J.* **2006**, *52* (7), 2310–2322. DOI: <https://doi.org/10.1002/aic.10847>
- [2] Y. Hirata, A. W. Nienow, I. P. T. Moore, *J. Chem. Eng. Jpn.* **1994**, *27* (2), 235–237. DOI: <https://doi.org/10.1252/jcej.27.235>
- [3] L. Doucet, G. Ascanio, P. A. Tanguy, *Chem. Eng. Res. Des.* **2005**, *83* (10), 1186–1195. DOI: <https://doi.org/10.1205/cherd.04254>

- 
- [4] L. Pakzad, F. Ein-Mozaffari, S. R. Upreti, A. Lohi, *Chem. Eng. Res. Des.* **2013**, *101*, 642–654. DOI: <https://doi.org/10.1016/j.ces.2013.07.027>
- [5] N. Ohmura, H. Masuda, S. Wang, *J. Chem. Eng. Jpn.* **2018**, *51* (2), 129–135. DOI: <https://doi.org/10.1252/jcej.17we149>
- [6] K. Kataoka, H. Doi, T. Kongo, M. Futagawa, *J. Chem. Eng. Jpn.* **1975**, *8* (6), 472–476. DOI: <https://doi.org/10.1252/jcej.8.472>
- [7] K. Kataoka, N. Ohmura, M. Kouzu, Y. Simamura, M. Okubo, *Chem. Eng. Sci.* **1995**, *50* (9), 1409–1416. DOI: [https://doi.org/10.1016/0009-2509\(94\)00515-5](https://doi.org/10.1016/0009-2509(94)00515-5)
- [8] M. Matsumoto, H. Masuda, R. Hubacz, T. Horie, H. Iyota, M. Shimoyamada, N. Ohmura, *Chem. Eng. Sci.* **2021**, *231*, 116270. <https://doi.org/10.1016/j.ces.2020.116270>
- [9] H. Masuda, T. Horie, R. Hubacz, N. Ohmura, *Chem. Eng. Res. Des.* **2013**, *91* (11), 2259–2264. DOI: <https://doi.org/10.1016/j.cherd.2013.08.026>
- [10] H. Masuda, R. Hubacz, M. Shimoyamada, N. Ohmura, *Chem. Eng. Technol.* **2019**, *42* (4), 859–866. DOI: <https://doi.org/10.1002/ceat.201800600>
- [11] X. Gao, B. Kong, M. Ramezani, M. G. Olsen, R. D. Vigil, *Int. J. Heat Mass Transf.* **2015**, *91*, 433–445. DOI: <https://doi.org/10.1016/j.ijheatmasstransfer.2015.07.125>
- [12] B. Haut, H. Ben Amor, L. Coulon, A. Jacquet, V. Halloin, *Chem. Sci. Eng.* **2003**, *58* (3–6), 777–784. DOI: [https://doi.org/10.1016/S0009-2509\(02\)00607-3](https://doi.org/10.1016/S0009-2509(02)00607-3)
- [13] H. Masuda, T. Horie, R. Hubacz, M. Ohta, N. Ohmura, *Rheol. Acta* **2017**, *56* (2), 73–84. DOI: <https://doi.org/10.1007/s00397-016-0987-7>
- [14] N. Ohmura, K. Kataoka, Y. Shibata, T. Makino, *Chem. Eng. Sci.* **1997**, *52* (11), 1757–1765. DOI: [https://doi.org/10.1016/S0009-2509\(97\)00012-2](https://doi.org/10.1016/S0009-2509(97)00012-2)
- [15] M. Wimmer, *J. Fluid Mech.* **1995**, *292*, 205–227. DOI: <https://doi.org/10.1017/S0022112095001492>
- [16] N. Ohmura, M. N. Noui-Mehidi, K. Sasaki, K. Kitajima, K. Kataoka, *J. Chem. Eng. Jpn.* **2004**, *37* (4), 546–550. DOI: <https://doi.org/10.1252/jcej.37.546>, [546550](https://doi.org/10.1252/jcej.37.546)
- [17] P. J. Carreau, *Trans. Soc. Rheol.* **1972**, *16*, 99–127. DOI: <https://doi.org/10.1122/1.549276>
- [18] M. N. Noui-Mehidi, *Exp. Therm. Fluid Sci.* **2005**, *29* (4), 447–456. DOI: <https://doi.org/10.1016/j.expthermflusci.2004.05.019>
- [19] R. Srinivasan, S. Jayanti, A. Kannan, *AIChE J.* **2005**, *51* (11), 2885–2898. DOI: <https://doi.org/10.1002/aic.10553>
- [20] M. N. Noui-Mehidi, N. Ohmura, K. Kataoka, *J. Fluids Struct.* **2002**, *16* (2), 247–262. DOI: <https://doi.org/10.1006/jfls.2001.0417>
- [21] Y. Zhang, L. Xu, D. Li, *Commun. Nonlinear Sci. Numer. Simul.* **2012**, *17* (1), 235–241. DOI: <https://doi.org/10.1016/j.cnsns.2011.05.021>
- [22] R. Hubacz, N. Ohmura, E. Dluska, *J. Food Process Eng.* **2013**, *36* (6), 774–785. DOI: <https://doi.org/10.1111/jfpe.12046>
- [23] P. V. Danckwerts, *Appl. Sci. Res. A.* **1952**, *3*, 279–296. DOI: <https://doi.org/10.1007/BF03184936>
- [24] T. X. Dinh, Y. Ogami, *J. Fluid Sci. Tech.* **2008**, *3* (2), 250–259. DOI: <https://doi.org/10.1299/jfst.3.250>
-

---

## Figure captions

**Figure 1.** Computational domain.

**Figure 2.** Rheological properties of fluids used in this study.

**Figure 3.** Comparison of (a) experimental and (b) numerical results at  $Re|_{\text{top}} = 160$ : (a) flow pattern visualized with aluminum flakes and (b) velocity vectors in the (x-z) plane. In both cases, seven pairs of Taylor vortices were observed.

**Figure 4.** Dependence of mesh number on velocity distribution 30 s after the start of the rotation of the inner cone at the middle of the gap along the axis:  $Re|_{\text{top}} = 200$  and  $\alpha = 8^\circ$ .

**Figure 5.** Effect of apex angle on velocity distribution 30 s after the start of the rotation of the inner cone in Newtonian and shear-thinning fluids. In each figure, the left and right sides correspond to the inner and outer cone (cylinder) surfaces, respectively.

**Figure 6.** Velocity distribution in the middle of the gap along the axis for  $Re_{\text{eff}}|_{\text{top}} = 200$  and  $n = 0.5$ . The velocity peak was confirmed to shift upward between  $t = 20$  and 30 s.

**Figure 7.** Effect of shear-thinning property ( $n$ ) on the normalized velocity of the upward motion of a Taylor cell.

**Figure 8.** Passive scalar transport with time at  $Re_{\text{eff}}|_{\text{top}} = 200$  and  $n = 0.3$ : (a) cylindrical ( $\alpha = 0^\circ$ ) and (b) conical ( $\alpha = 8^\circ$ ) systems. In each figure, the left and right sides correspond to the inner and outer cone (cylinder) surfaces, respectively.

**Figure 9.** Effect of shear-thinning property ( $n$ ) on passive scalar transport at  $Re|_{\text{top}}$  ( $Re_{\text{eff}}|_{\text{top}}$ ) = 200 in a conical system ( $\alpha = 8^\circ$ ):  $t^* =$  (a) 2,340 and (b) 6,200. In each figure, the left and right sides correspond to the inner and outer cone (cylinder) surfaces, respectively.

**Figure 10.** Distributive mixing efficiency as a function of the non-dimensional time ( $t^*$ ) in each fluid system at  $Re|_{\text{top}}$  ( $Re_{\text{eff}}|_{\text{top}}$ ) = 200.

## Entry for the Table of Contents

**Type of Article:** A conical Taylor–Couette flow was utilized as a mixing device. A global convection (i.e. meridional flow) intensifies the global mixing keeping good local mixing within Taylor cells. The meridional flow was found to be enhanced with increasing shear-thinning. Thus, global mixing with shear-thinning fluids was promoted by the enhanced meridional flow compared with that of Newtonian fluids.

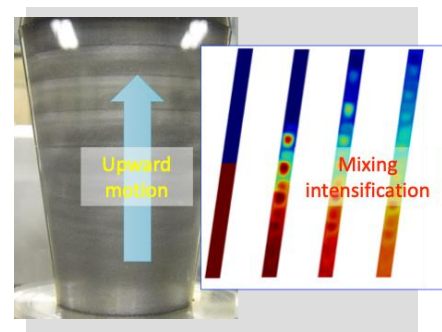
### Title

**Global convection characteristics of conical Taylor–Couette flow with shear-thinning fluids**

H. Masuda\*, H. Iyota, N. Ohmura

*Chem. Eng. Technol.* **20XX**, *XX* (X),

XXXX...XXXX



((Pls. indicate if Supporting Information are available))